Molecular Surface Quantification of Multi-Functionalized Gold Nanoparticles Using UV-visible Absorption Spectroscopy Deconvolution

Jordan C. Potts[a], Akhil Jain[b], David B. Amabilino[c], Frankie J. Rawson[b]* and Lluïsa Pérez-García[a,d,e]*

[a] Division of Advanced Materials and Healthcare Technologies, School of Pharmacy, University of Nottingham, Nottingham NG7 2RD, UK

[b] Bioelectronics Laboratory, Division of Regenerative Medicine and Cellular Therapies, School of Pharmacy, University of Nottingham, Biodiscovery Institute, Nottingham NG7 2RD, UK

[c] Institut de Ciència de Materials de Barcelona (ICMAB), CSIC, Carrer dels Til·lers, Campus Universitari, 08193 Cerdanyola del Vallès, Catalunya, Spain

[d] Departament de Farmacologia, Toxicologia i Química Terapèutica, Facultat de Farmàcia i Ciències de l'Alimentació, Universitat de Barcelona, 08028 Barcelona, Spain

[e] Institut de Nanociència i Nanotecnologia UB (IN2UB), Universitat de Barcelona, 08028 Barcelona, Spain

KEYWORDS: Gold Nanoparticles, Multifunctional, Cytochrome C, Zinc Porphyrin, Characterization

ABSTRACT: Multi-functional gold nanoparticles (AuNPs) are of great interest, owing to their vast potential for use in many areas including sensing, imaging, delivery, and medicine. A key factor in determining the biological activity of multi-functional AuNPs is the quantification of surface conjugated molecules. There has been a lack of accurate methods to determine this for multi-functionalized AuNPs. In this work, we address this limitation by using a new method based on deconvolution and Levenberg-Marquardt algorithm fitting of UV-visible absorption spectrum to calculate the precise concentration and number of cytochrome C (Cyt *C*) and Zinc Porphyrin (Zn Porph) bound to each multi-functional AuNP. Dynamic light scattering (DLS), Zeta potential measurements, and Transmission Electron Microscopy (TEM) were used to confirm the functionalization of AuNPs with Cyt *C* and Zn Porph. Despite the overlapping absorption bands of Cyt *C* and Zn Porph this method was able to reveal the accurate concentration and number of Cyt *C* and Zn Porph molecules attached per AuNP. Furthermore, using this method we were able to identify unconjugated molecules, suggesting the need for further purification of the sample. This guide provides a simple and effective method to quickly quantify molecules bound to AuNPs, giving users accurate and valuable information, especially for applications in drug delivery and biosensors.

AuNPs are a class of nanomaterials that have gained broad research interest due to their attractive properties such as optical, chemical inertness, facile synthesis, and surface chemistry. These properties make AuNPs ideal for biological and medical applications, including use in biosensors, genomics, targeted delivery of drugs, DNA and antigens, optical bioimaging and clinical chemistry, to name but a few.[1-4]

The ability to functionalize AuNPs with molecules has led to an interest in designing more complex systems with multiple molecule types conjugated to each AuNP, known as multi-functionalized AuNPs. These multi-functionalized AuNPs have a significant advantage over AuNPs conjugated with just one type of molecule as they can be used for more broad applications.[5] An example of multi-functionalized AuNPs is in drug delivery systems, where a targeting agent and drug are conjugated to the surface of the particle to direct the effect of the drug to a specific cell type or region.[6-8] Another example would be in cancer treatments where multi-functionalized AuNPs can deliver two anticancer drugs to the same targeted tissue simultaneously.[9]

The concentration of conjugated molecules on the surface of the AuNPs is an important factor that determines its nano-bio interactions and eventually its biological function. In pharmaceutical applications, the concentration of the conjugated molecules is a significant factor in modulating drug dose thresholds. In biosensing, the minimum concentration of analyte that can be detected is known as its limit of detection or sensitivity.[10] Accurately knowing the working concentrations and how sensitive a biosensor is essential to its accurate function. Consequently, there is a need to develop a simple, robust, and fast analytical method to facilitate surface quantification of AuNPs functionalized with more than one molecule. We have recently reported on the development of a multi-functional AuNP system functionalized with Cyt *C* for cell-induced apoptosis. Cyt *C* is a biomolecule of interest due to its redox properties that makes it useful for biosensing as well as its ability to induce apoptosis, lending it to applications in

drug delivery. [11-13] UV-visible absorption spectroscopy was used to quantitate the presence Cyt *C* on AuNPs functionalized with ligands of varying electrostatic charge.[14] Also, the quantitation of the presence of monolayers or multilayers was important to know when considering the concentration of drugs or biomolecules conjugated to AuNPs as a multilayer may interfere with their function, leading to an inaccurate representation of drug/biomolecule delivery or activity.

The concentration of biomolecules on functionalized AuNPs is commonly determined using bioassays suhch as ELISA, or less common techniques such as ToF-SIMS.[15, 16] The analytical methodology to determine the exact concentration of each functional molecule in a multifunctionalized material is not often thoroughly described. Furthermore, analysis of multi-functionalized AuNPs by UV-visible absorption spectroscopy is complicated by the molecular complexity caused, for example, by similarity in the absorption spectrum of the conjugated molecules such as porphyrins and proteins like Cyt *C* that could lead to erroneous calculated numbers.

To address this problem, we report on a new analysis protocol to quantitate a model multi-functionalized AuNP system that would allow us to accurately calculate the concentration of different molecules attached to the surface of AuNPs. Initially, AuNPs were synthesized and functionalized with Zn Porph and Cyt C. The concentration of the molecules conjugated to AuNPs could not be accurately determined due to overlapping absorption spectra. A method was then devised to deconvolute the merged absorption spectra of the two types of conjugated molecules using CASA-XPS. This enabled accurate identification of the peak heights of each type of conjugated molecule so the concentrations could be calculated for each type of molecule. This method can be used as a guide by the researchers to tailor binding parameters for obtaining multi-functionalized AuNPs for the desired application.

Experimental Section

Materials

Equine heart cytochrome *C* (Cyt *C*) (≥ 95%), *N*-(3-dimethylaminopropyl)-*N*′-ethylcarbodiimide hydrochloride (EDC), gold(III) chloride trihydrate ($HAuCl_4 \cdot 3H_2O$) (99.99%), thiol-PEG-carboxyl (HS-PEG-COOH) (2000 Da), 2-(*N*-morpholino)ethanesulfonic acid, 4-morpholineethanesulfonic acid monohydrate (MES monohydrate) (≥99.0%), *N*-hydroxysuccinimide (NHS) (98%), sodium citrate tribasic dihydrate (99%) were purchased from Sigma Aldrich. 5-(4-Aminophenyl)-10,15,20-tris-(4-sulfonatophenyl)porphyrin (Porph) and Zinc(II) 5-(4-aminophenyl)-10,15,20-tris-(4-sulfonatophenyl)porphyrin (Zn Porph) were purchased from Porphychem, France. Milli-Q® water at a resistivity of 18.2 MΩ provided by Milli-Q® direct water purification system was used for experiments.

Synthesis of 20 nm citrate capped AuNPs (cit-AuNPs)

1 mL of $HAuCl_4.3H_2O$ (39.38 mg, 0.1 mol) was added to 89 mL of ultrapure water and was brought to boil under constant stirring. Aqueous sodium citrate solution (38.8 mM, 10 mL) was rapidly added to the boiling solution causing a colour change from yellow to burgundy. The solution was boiled for 10 minutes before allowing it to cool down at room temperature under stirring. The solution was then filtered using a 0.22 μm nylon filter to remove any large aggregates, leaving monodispersed cit-AuNPs.

Functionalization of 20 nm cit-AuNPs with PEG, Cyt *C* and Zn Porph

A 1 mL solution of aqueous HS-PEG-COOH (2000 Da, 1 mM) was added to 20 mL of cit-AuNPs under stirring and left overnight. The following day the solution was washed twice using centrifugation at 13,400 rpm for 30 minutes to form a pellet of AuNP functionalized with PEG-COOH (AuNP-PEG). The pellet was then resuspended in ultrapure water and stored at 4°C until further use.

For covalent conjugation of Cyt *C* and Zn Porph, a fresh EDC/NHS mix solution was made by adding EDC (19.17 mg, 100 μmol) and NHS (23 mg, 200 μmol) in MES buffer (pH 5). A total of 100μL of EDC/NHS mix was added to the 1 mL solution of AuNP-PEG and was left stirring for 1 hour. The solution was then centrifuged at 13,400 rpm for 30 minutes to form a pellet of the AuNP with activated PEG-COOH. To this pellet Cyt *C* (1 mL, 200 μM) and Zn Porph (1 mL, 200 μM) were added under constant stirring (in AuNP-PEG-Cyt *C* only Cyt C was added, and in AuNP-PEG-Zn Porph only Zn Porph was added). The solution was stirred for 24 hours followed by three cycles of centrifugation at 13,400 rpm to remove any unbound Cyt *C* and Zn Porph. The obtained pellet was resuspended in 1 mL of water to yield a monodispersed sample of AuNP-PEG-Cyt *C*/Zn Porph.

Deconvolution modelling of Cyt C and Zn Porp conjugated to AuNPs

Deconvolution of UV-visible absorption absorption spectrum confirming the binding of Cyt *C* and Zn Porph was performed using CASA-XPS. The absorption spectra of the chosen samples were imported into CASA-XPS as text files. The X-axis was then reversed to represent the UV-visible absorption absorption spectrum is habitually represented. The region of interest was then selected using the regions tool, and then the background setting was changed to 'linear' as it closely represents how the spectra would look without the conjugated molecules. The convoluted peaks in the spectra were then found using the components tab, by adding the components that were thought to be in the region. The components were then fitted to the spectra using Levenberg-Marquardt algorithm LN (LN-MIE-Gans) fitting. The resulting spectra data was copied to Microsoft Excel before being added to GraphPad Prism 9 for analysis.

LN-MIE-Gans modelling of cit-AuNPs and multi-functionalized AuNPs

Model fitting on AuNP spectra to predict their size was conducted on Wolfram Mathematica using the LNMG Fit 1.0 model obtained from the literature.[17]

Instruments

Ultraviolet-Visible (UV-visible absorption) absorption spectra were obtained using a Varian Cary 50 bio-UV-visible absorption spectrophotometer. Centrifugation was performed on a Spectrafuge 24D. The transmission electron microscope (TEM) images were captured using JEOL FX 2000 TEM at 200 kV. The histogram of AuNP size distribution was determined from the TEM images using ImageJ® software. Dynamic light scattering (DLS) and Zeta potential experiments were conducted on a Malvern Zetasizer nano.

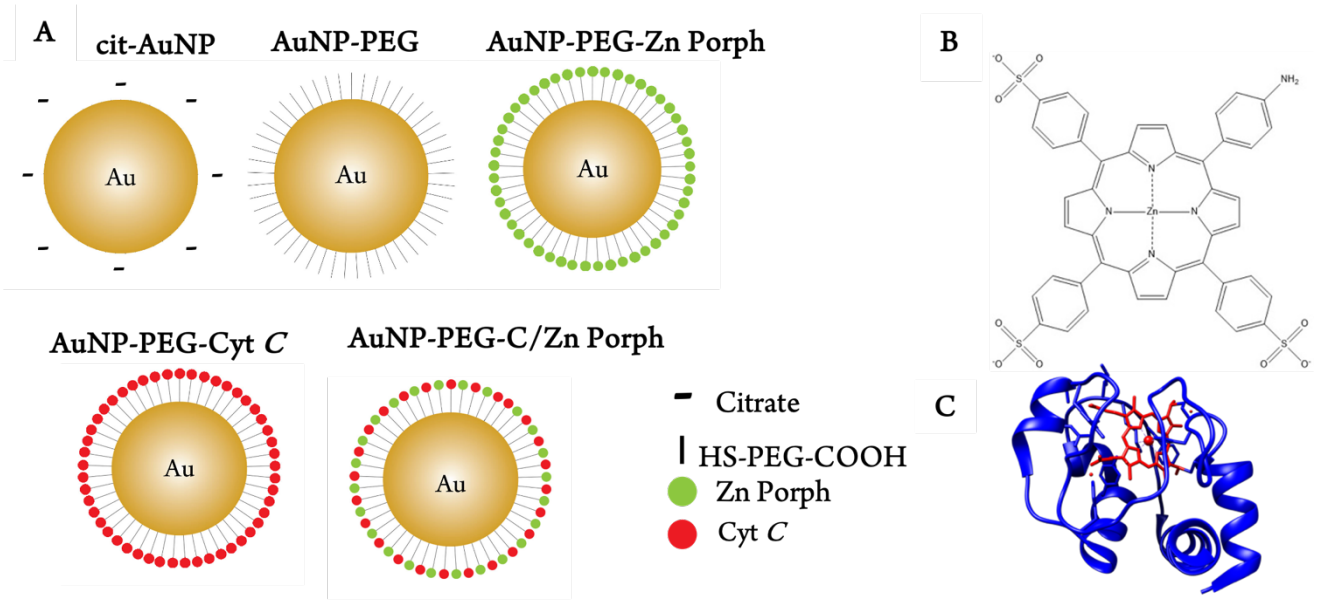

Figure 1. Schematic representation of cit-AuNPs as synthesised and when functionalized with thiol-PEG-carboxylic, Cytochrome *C* (Cyt *C*) and Zinc(II) 5-(4-aminophenyl)-10,15,20-tris-(4-sulfonatophenyl)porphyrin (Zn Porph) **(A)**. Structure of Zn Porph **(B)**. 3D structure crystal of Cyt *C* made from PDB (1 HRC) using Chimera (version 1.16) with blue representing amino acid residues and red representing the porphyrin Heme ring **(C)**.

Results and Discussion

The freshly prepared cit-AuNPs were functionalized with the HS-PEG-COOH. Carbodiimide coupling chemistry was then employed to covalently conjugate Cyt *C* and Zn Porph (AuNP-PEG-Cyt *C*/Zn Porph). Schematic representations of cit-AuNP, AuNP-PEG, AuNP-PEG-Zn Porph, AuNP-PEG-Cyt *C* and AuNP-PEG-Cyt *C*/Zn Porph are shown in Figure 1A. The chemical structure of Zn Porph is represented in Figure 1B. The 3-D structure of Cyt *C* is shown in Figure 1C with the amino acid residues represented in blue and the heme porphyrin ring represented in red.

It was important to begin with to physically characterise the particles to allow later quantification. We initially perform light scattering techniques to assess the change in hydrodynamic diameter (hd) and zeta potential of cit-AuNPs, AuNPs-PEG, and AuNP-PEG-Cyt C/Zn Porph samples. The length of the fully extended HS-PEG-COOH (2000 Da) is ca. 7.9 nm, while the diameter of Cyt *C* is ca. 3.4 nm and the diameter of of Zn Porph is around ca. 1.6 nm (calculated using ChemDraw3D).[18] The hydrodynamic diameters (h_d) of cit-AuNPs, AuNP-PEG and AuNP-PEG-Cyt *C*/Zn Porph were measured using DLS (Figure 2A). This analysis revealed a difference in the h_d of the Cit-AuNPs from 19.6±1.0 nm to 33.54±0.50 nm in AuNP-PEG and to 38.9±1.1 nm for AuNP-PEG-Cyt *C*/Zn Porph, suggesting successful conjugation. Zeta potential measurements are useful in providing an insight into the change in surface chemistry by measuring the surface charge.[14] Therefore, the zeta potential was used to confirm the successful conjugation of molecules to AuNPs. The zeta potential measurement of cit-AuNPs was recorded to be -36.77±2.33 mV which a slightly lower value of to -30.77 ±1.4 mV for AuNP-PEG and +14.7 ±0.9 mV for AuNP-PEG-*C* (Figure 2C). On the other hand, the zeta potential values of AuNP-PEG-Zn Porph as -27.3±0 mV vs AuNP-PEG indicates the successful conjugation of Zn Porph. Cyt *C* is known to have a positive zeta potential measurement which is exhibited on the AuNP-PEG-Cyt *C* samples, confirming successful conjugation of Cyt *C* on PEG functionalized AuNPs.[14] Similarly, the change in zeta potential values of -27.3±0 mV vs AuNP-PEG indicates the successful conjugation of Zn Porph. Cyt *C* is known to have a positive zeta potential measurement which is exhibited on the AuNP-PEG-Cyt *C* samples, confirming successful conjugation of Cyt *C* on PEG functionalized AuNPs.[14] Similarly, the change in zeta potential values of -27.3 mV in AuNP-PEG-Zn Porph to +10.8 ±0.2 mV for AuNP-PEG-C/Zn Porph samples confirms the successful conjugation of both Cyt *C* and Zn Porph to AuNPs-PEG.

TEM was carried out to analyse the morphology, aggregation, and size of surface functionalized AuNPs. TEM analysis revealed that the AuNP-PEG-Cyt *C* /Zn Porph particles are monodisperse and the functionalization process does not cause any aggregation (Figure 2B). Furthermore, the cumulative frequency graph (inset of Figure 2B) reveals a mean average diameter of AuNP-PEG- Cyt *C* /Zn Porph samples to be around 19.15±2.12 nm (Gaussian fit). The size discrepancy between TEM and DLS is because TEM. DLS measures the hydrodynamic diameter of particles in suspension and therefore can differentiate between the Cit-AuNPs and the multi-functionalized AuNPs.

Further to confirm the successful conjugation of Cyt *C* and Zn Porph to AuNPs, they were characterized using UV-visible absorption absorption spectroscopy. UV-visible absorption spectroscopy is a widely used technique used when working with AuNPs as the absorption spectrum can determine both their size and concentration.[19] The maximum absorbance of the surface plasmon resonance (SPR) peak in the spectra, located between 500 and 600 nm, is indicative of their size. Once the size and the extinction coefficient of the AuNPs are known, their concentration can be calculated using the Beer-Lambert law.[19, 20, 21]

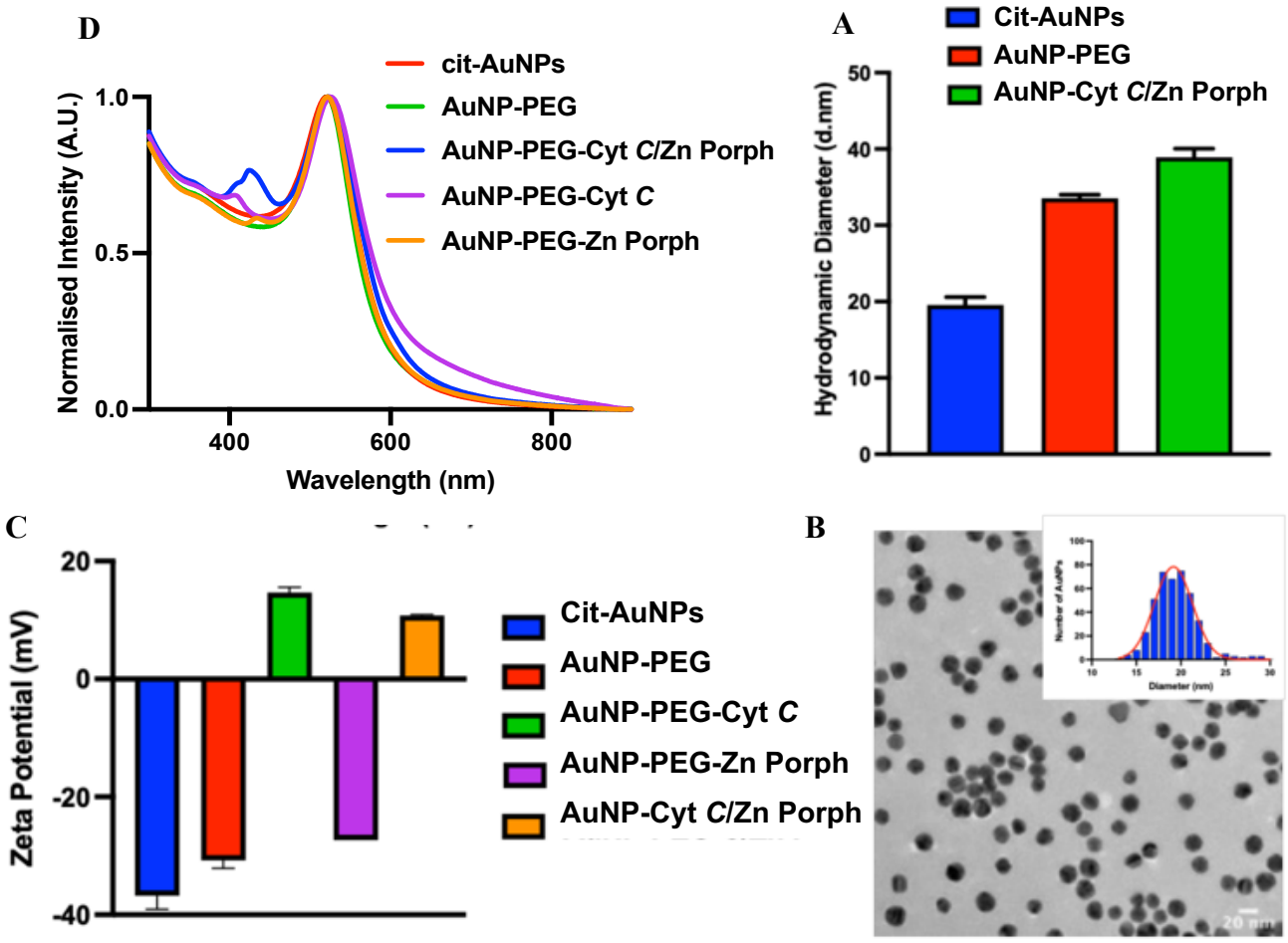

Figure 2. Physico-chemical characterization AuNPs functionalized with Cyt *C* and Zn Porph. UV-visible absorption spectroscopy **(A),** DLS **(B)**, Zeta Potential measurements **(C),** and TEM image and cumulative frequency graph of 20 nm AuNP-PEG-Cyt *C*/Zn Porph **(D)**

On the other hand, porphyrins are commonly conjugated in nanomaterials for fluorescent tagging and photodynamic therapy. [22-25] The UV-visible absorption spectra of all AuNPs synthesized in this work are reported in Figure 2D. Their UV-visible absorption spectra reveal that the SPR peak of the AuNPs remains in the same position at 521 nm for all the samples except AuNP-PEG-Cyt *C*, in which SPR band is red-shifted to 525 nm compared to cit-AuNPs (521 nm), indicating successful functionalization of Cyt *C* onto AuNP-PEG. Moreover, full width half maximum (FWHM) of the SPR peak increased in all the functionalized AuNP samples when compared to the spectrum of cit-AuNPs, suggesting an increase in polydispersity of the functionalized AuNPs which could be the result of agglomerates which could form in the colloidal dispersions. Cit-AuNPs and AuNPs-PEG do not show any absorption peaks other than the SPR., whereas free Cyt *C* and Zn Porph exhibit additional peaks, and their UV-visible absorption absorption spectra are shown in Figure S1A. The Soret band peaks at 408 nm and 415 nm are for oxidised (Cyt *C* Ox) and reduced Cyt *C* (Cyt *C* Red), respectively, which aligns with literature values.[26] The absorption peak at 423 nm corresponds to Zn Porph (Figure S1A). After conjugation to AuNPs, the Soret band peak of Cyt *C* was located at 410 nm, suggesting that the Cyt *C* conjugated to the AuNPs exists in both oxidized and reduced forms. While the Zn Porph Soret band is evident at 430 nm, which is red shifted when compared to free Zn Porph in solution at 423 nm. This red shift in Zn Porph peak after conjugation to AuNPs could be attributed to J-type aggregation formed between neighbouring chromophores (in this case Zn Porph) attached close to each other in a nanoparticle.[27] It is evident from Figure 2A that in multifunctional AuNP-PEG-Cyt *C*/Zn Porph samples the Soret band peaks of Cyt *C* and Zn Porph overlap, consequently the exact peak of each of the components is difficult to determine. Importantly, this poses the risk of erroneous calculation to determine the accurate concentrations of these molecules. The overlapping spectra of Cyt *C* Ox and Zn Porph (Figure S1B) and Cyt *C* Red and Zn Porph (Figure S1C) free in solution supports the spectrum depicted in Figure 2A, showing how the absorbance peaks convolute and make accurate peak determination impossible. Therefore, the deconvolution of the overlapping spectra of Cyt *C* Ox and Zn Porph and Cyt *C* Red and Zn Porph (Figure S1D and Figure S1E) is essential as it allows the hidden peaks to be revealed, and therefore the absorbance of each peak to be identified for further quantification purpose.

The spectral overlap of the Soret band of Cyt *C* and Zn Poprh (Figure S1A) prevents the identification of individual Soret

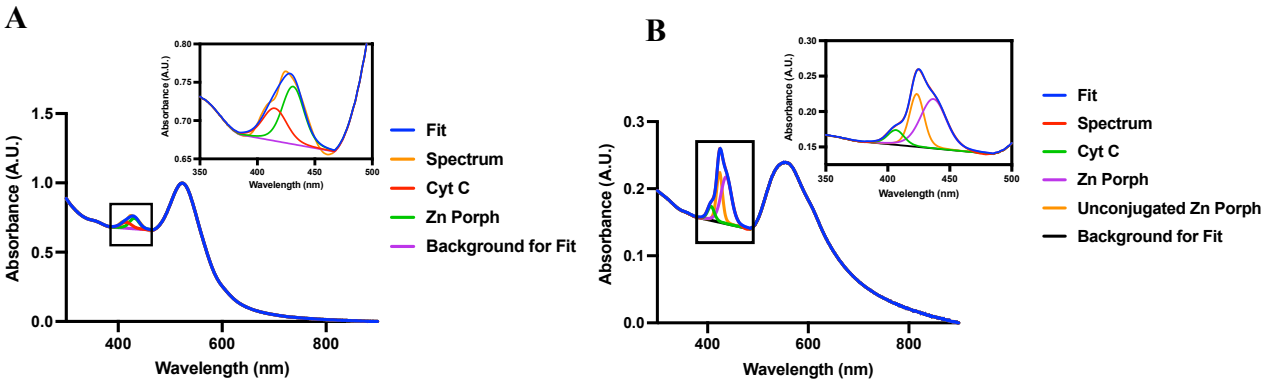

Figure 3. Deconvolution of the Ultraviolet-Visible spectra of AuNP-PEG-C/Zn Porph with **(A)** 2 fitted components in AuNP-PEG-Cyt *C*/Zn-Porph samples and **(B)** 3 fitted component in AuNP-PEG-Cyt *C*/Zn-Porph-S2

peak heights in AuNP-PEG-Cyt *C*/Zn Porph. Therefore, deconvolution of the Soret band of AuNP-PEG-Cyt *C* /Zn Porph was conducted to accurately find the contributions of Cyt *C* and Zn Porph in the functionalized AuNP samples. (Figure 3A). The Soret band was selected as a region of interest in CASA-XPS and two components (one for Cyt *C* and the other one for Zn Porph) were selected to be fitted in the AuNP-PEG-Cyt *C* /Zn Porph absorption spectrum shown in Figure 3A. These were located at 415 nm, attributed to Cyt *C*, and at 430 nm for Zn Porph. The components were fitted using the Levenberg-Marquardt algorithm fitting which resulted in a good fit with a residual standard deviation (RSD) of 0.006. Therefore, the good fit confirms that only two components are located within the peak and that the deconvolution accurately can determine the heights of the hidden peaks.

To confirm the accuracy of the analysis technique another sample/batch of Cyt C and Zn Porph functionalized sample (AuNP-PEG-Cyt *C*/Zn Porph-S2) with a more complex Soret band peak was deconvoluted (Figure 3B). When the Soret band of Figure 3B is compared to Figure 3A, it appears as a different shape with shoulders on each side of the peak. In this case, fitting the deconvoluted spectrum with just two components resulted in a large RSD suggesting the presence of another component. Therefore, the third component at 423 nm which corresponds to the absorption peak of free unconjugated Zn Porph (Fig S1A) was added to improve the fit. The fitting resulted in an RSD of 0.002 (Figure 3B). The inclusion of a third component supposes that free/unconjugated Zn Porph is still present in the solution together with Zn Porph conjugated to AuNPs. Therefore, suggesting further purification of the sample is required. Interestingly, the formation of Zn Porph J-aggregates can also be identified using this method, which is of great importance as the fluorescence properties of porphyrins depend on their aggregation state and local environment. [28, 29] This can also be done by deconvoluting the UV-visible absorption absorption spectra of free Cyt *C* OX and Zn Porph in water (Figure S1D). Based on the above observations it is evident that this analysis is essential and should be performed regularly to every batch of samples together with UV-visible absorption spectroscopy for accurate quantification of bound molecules, especially in applications such as drug delivery where UV-visible absorption is often used to quantify surface conjugated molecules.

To further the impact of this method we then calculated the concentration of surface functionalized molecules on AuNPs for both samples of AuNP-PEG-Cyt *C*/Zn Porph in Figure 3A and Figure 3B. The number of each bound molecule was calculated from the UV-visible absorption absorption spectrum shown in Figures 3A and 3B using the Beer-Lambert law. The extinction coefficient of the ca. 20 nm AuNPs (5.41×10^{8} M^{-1} cm^{-1}) was divided by each of the absorbance values at the minimum absorbance value between the SPR peaks and the conjugated molecule peaks. Based on the above method the calculated concentrations of 1.21 nM and 0.26 nM were obtained for samples (AuNP-PEG-Cyt c/Zn Poprh and AuNP-PEG-Cyt c/Zn Poprh S2, respectively) Figures 3A and B respectively can then be multiplied by Avogadro's constant (6.022×10^{23}) to give 7.30×10^{14} and 1.55×10^{14} AuNPs per litre.

The number of Cyt *C* and Zn Porph molecules per litre can also be found by first calculating their concentration and subsequently the number of molecules per AuNP. For the concentration, the height of the deconvoluted peaks was found by subtracting the background from the spectra. The absorbance peak heights were then divided by the extinction coefficients of Cyt *C* (101600 M^{-1} cm^{-1}) and Zn Porph (57940 M^{-1} cm^{-1}, calculated from a concentration curve in Figure S3), resulting in the bound concentrations.[30] The concentration of Cyt *C* for the AuNP-PEG-Cyt c/Zn Poprh sample (Figure 3A) was calculated to be 0.42 µM, which corresponds to 2.53×10^{17} Cyt *C* molecules per litre. Similarly, the concentration of Zn Porph for AuNP-PEG-Cyt c/Zn Poprh sample (Figure 3A) was calculated to be 1.30 µM, with a subsequent 7.83×10^{17} Zn Porph molecules per litre. By dividing the number of molecules of Cyt *C* and Zn Porph per litre by the number AuNPs per litre, the quantity of each molecule was calculated to be 346 and 1073, respectively. The AuNP concentration of the AuNP-PEG-Cyt c/Zn Poprh-S2 (Figure 3B) was calculated to be 0.26 nM, with 1.55×10^{14} AuNPs per litre. The concentrations of Cyt *C* and Zn Porph were calculated to be 0.40 µM and 1.16 µM, equating to 2.4×10^{17} and 6.99×10^{17} molecules per litre respectively. Thus, the number of molecules bound to each AuNP was calculated to be 1545 Cyt *C* and 4500 Zn Porph. The Zn Porph free solution in this sample was also calculated to have a concentration of 1.11 µM. The quantity of conjugated molecules in Figure 3B is over four-fold the quantity of conjugated in Figure 3A, suggesting that the Zn Porph free in solution is hindering the accurate determination of the number of molecules bound to the AuNPs. Deconvolution of peaks on multi-functional AuNPs, therefore, provides users with valuable information about the quality and concentration of their conjugated molecules, while also providing insight into whether their material needs to be purified further.

To prove the robustness and reproducibility of this method another example of Soret band deconvolution was conducted on the sample with a closer overlap in 50 nm AuNPs (Figure S4A). The Soret band of 50 nm cit-AuNPs functionalized with HS-PEG-COOH, Cyt *C* and a non-metalated porphyrin (Porph, structure in Figure S4B) appears as a single peak. The maximum Soret band absorbance of Porph at 415 nm shows a greater overlap with reduced Cyt *C* (λ_{max} = 415 nm) (Figure S4C) than that Zn Porph at 423 nm, therefore individual component concentrations cannot be calculated from the convoluted peak. The deconvolution enables the concentrations of Cyt C and Porph mixed free in solution (Figure S4D) to be calculated as 2.12 μM and 2.65 μM respectively, closely matching the 2.5 μM theoretical concentration of the prepared solutions. For 50 nm AuNP-PEG-Cyt *C*/Porph the concentrations of Cyt *C* and Porph were determined to be 0.11 μM and 0.17 μM respectively. The coverage of Cyt *C* and Porph per AuNP was 23,259 and 35,168 respectively (Table S2). The higher number of molecules per AuNP is due to the lower concentration of AuNPs in the sample and their larger diameter.

Deconvolution was not conducted on the peak between 500 and 600 nm, as this region was attributed to the SPR peak of the AuNPs. The LN-MIE-Gans model fitting taken from literature of 20 nm AuNPs evidences this (Figure S5A), as it can predict the radius of the AuNPs based on the fit of the model to the spectra (Figure S5B).[17] For the spectrum of 20 nm cit-AuNPs, the radius is predicted to be 10 nm with a resultant predicted diameter of 20 nm. The predicted diameter correlates with those calculated previously from the TEM at 19.15±2.12 nm and DLS at 19.57±1.03 nm (cit-AuNPs), therefore it can be assumed that the only region of interest for deconvolution in these examples is within the Soret band region.

Conclusion

In conclusion, we have established a simple, robust, and reproducible method to accurately quantify the concentration and the exact number of molecules that are bound to AuNPs. Deconvolution of UV-visible absorption absorption spectra is highly recommended that can be used in collaboration with DLS, Zeta potential and TEM to build an accurate understanding of the quantity and nature of conjugated molecules on multi-functionalized AuNPs. This method of accurately determining the concentration of each molecule bound to multi-functionalized AuNPs could be used by researchers from various disciplines. For instance, to tailor the material surface and binding concentration based on desired application without misinterpreting the binding concentration.

ASSOCIATED CONTENT

Supporting Information

AUTHOR INFORMATION

Corresponding Author

Frankie.rawson@notitngham.ac.uk: Division of Regenerative Medicine and Cellular Therapies, School of Pharmacy, University of Nottingham, Nottingham NG7 2RD, UK

mlperez@ub.edu - Departament de Farmacologia, Toxicologia i Química Terapèutica, Universitat de Barcelona, Barcelona, Spain.

Author Contributions

JP performed the experimental work. JP and AJ methodology. AJ lab training and monitoring. JP wrote the original manuscript. AJ, DBA, LPG and FJR contributed to editing and writing. DBA, LPG and FJR conceptualized the project. AJ, DBA, LPG and FJR supervised the project. JP was the lead on data analysis. AJ, DBA, LPG and FJR reviewed the data analysis.

ACKNOWLEDGMENT

This work was supported by the Engineering and Physical Sciences Research Council grant numbers EP/R004072/1. LPG work was also supported by project PID2020-115663GB-C3-2 funded by MCIN/AEI/10.13039/501100011033.

REFERENCES

1. Dykman, L. A.; Khlebtsov, N. G., Gold nanoparticles in biology and medicine: recent advances and prospects. *Acta naturae* **2011,** *3* (2), 34-55.
2. Nejati, K.; Dadashpour, M.; Gharibi, T.; Mellatyar, H.; Akbarzadeh, A., Biomedical Applications of Functionalized Gold Nanoparticles: A Review. *Journal of Cluster Science* **2022,** *33* (1), 1-16.
3. Duan, L.; Ouyang, K.; Xu, X.; Xu, L.; Wen, C.; Zhou, X.; Qin, Z.; Xu, Z.; Sun, W.; Liang, Y., Nanoparticle Delivery of CRISPR/Cas9 for Genome Editing. *Front Genet* **2021,** *12*, 673286-673286.
4. Trabbic, K. R.; Kleski, K. A.; Barchi, J. J., Stable Gold-Nanoparticle-Based Vaccine for the Targeted Delivery of Tumor-Associated Glycopeptide Antigens. *ACS Bio & Med Chem Au* **2021,** *1* (1), 31-43.
5. Mieszawska, A. J.; Mulder, W. J. M.; Fayad, Z. A.; Cormode, D. P., Multifunctional gold nanoparticles for diagnosis and therapy of disease. *Molecular pharmaceutics* **2013,** *10* (3), 831-847.
6. Hosta-Rigau, L.; Olmedo, I.; Arbiol, J.; Cruz, L. J.; Kogan, M. J.; Albericio, F., Multifunctionalized Gold Nanoparticles with Peptides Targeted to Gastrin-Releasing Peptide Receptor of a Tumor Cell Line. *Bioconjug Chem* **2010,** *21* (6), 1070-1078.
7. Mohamed, M. S.; Veeranarayanan, S.; Poulose, A. C.; Nagaoka, Y.; Minegishi, H.; Yoshida, Y.; Maekawa, T.; Kumar, D. S., Type 1 ribotoxin-curcin conjugated biogenic gold nanoparticles for a multimodal therapeutic approach towards brain cancer. *Biochimica et Biophysica Acta (BBA) - General Subjects* **2014,** *1840* (6), 1657-1669.
8. Taghdisi, S. M.; Danesh, N. M.; Lavaee, P.; Emrani, A. S.; Hassanabad, K. Y.; Ramezani, M.; Abnous, K., Double targeting, controlled release and reversible delivery of daunorubicin to cancer cells by polyvalent aptamers-modified gold nanoparticles. *Mater Sci Eng C Mater Biol Appl* **2016,** *61*, 753-61.
9. Al-Shakarchi, W.; Alsuraifi, A.; Abed, M.; Abdullah, M.; Richardson, A.; Curtis, A.; Hoskins, C., Combined Effect of Anticancer Agents and Cytochrome C Decorated Hybrid Nanoparticles for Liver Cancer Therapy. *Pharmaceutics* **2018,** *10* (2), 48.
10. Bhalla, N.; Jolly, P.; Formisano, N.; Estrela, P., Introduction to biosensors. *Essays Biochem* **2016,** *60* (1), 1-8.
11. Manickam, P.; Kaushik, A.; Karunakaran, C.; Bhansali, S., Recent advances in cytochrome c biosensing technologies. *Biosensors and Bioelectronics* **2017,** *87*, 654-668.
12. Guo, C.; Wang, J.; Chen, X.; Li, Y.; Wu, L.; Zhang, J.; Tao, C.-a., Construction of a Biosensor Based on a Combination of Cytochrome c, Graphene, and Gold Nanoparticles. *Sensors* **2018,** *19* (1).
13. Delinois, L. J.; De León-Vélez, O.; Vázquez-Medina, A.; Vélez-Cabrera, A.; Marrero-Sánchez, A.; Nieves-Escobar, C.; Alfonso-Cano, D.; Caraballo-Rodríguez, D.; Rodriguez-Ortiz, J.; Acosta-Mercado, J.; Benjamín-Rivera, J. A.; González-González, K.; Fernández-Adorno, K.; Santiago-Pagán, L.; Delgado-Vergara, R.; Torres-Ávila, X.; Maser-Figueroa, A.; Grajales-Avilés, G.; Méndez, G. I. M.; Santiago-Pagán, J.; Nieves-Santiago, M.; Álvarez-Carrillo, V.; Griebenow, K.; Tinoco, A. D., Cytochrome c: Using Biological Insight toward Engineering an Optimized Anticancer Biodrug. *Inorganics* **2021,** *9* (11), 83.
14. Jain, A.; Trindade, G. F.; Hicks, J. M.; Potts, J. C.; Rahman, R.; Hague, R. J. M.; Amabilino, D. B.; Pérez-García, L.; Rawson, F. J.,

Modulating the biological function of protein by tailoring the adsorption orientation on nanoparticles. *Journal of Colloid and Interface Science* **2021,** *587*, 150-161.

15. Zhang, M.; Zheng, J.; Wang, J.; Xu, J.; Hayat, T.; Alharbi, N. S., Direct electrochemistry of cytochrome c immobilized on one dimensional Au nanoparticles functionalized magnetic N-doped carbon nanotubes and its application for the detection of H2O2. *Sensors and Actuators B: Chemical* **2019,** *282*, 85-95.

16. Ju, S.; Yeo, W.-S., Quantification of proteins on gold nanoparticles by combining MALDI-TOF MS and proteolysis. *Nanotechnology* **2012,** *23* (13), 135701 1-7.

17. Amendola, V.; Meneghetti, M., Size Evaluation of Gold Nanoparticles by UV−vis Spectroscopy. *The Journal of Physical Chemistry C* **2009,** *113* (11), 4277-4285.

18. Garrido, C.; Galluzzi, L.; Brunet, M.; Puig, P. E.; Didelot, C.; Kroemer, G., Mechanisms of cytochrome c release from mitochondria. *Cell Death And Differentiation* **2006,** *13*, 1423.

19. Haiss, W.; Thanh, N. T. K.; Aveyard, J.; Fernig, D. G., Determination of Size and Concentration of Gold Nanoparticles from UV−Vis Spectra. *Analytical Chemistry* **2007,** *79* (11), 4215-4221.

20. Grimsley, G. R.; Pace, C. N., Spectrophotometric determination of protein concentration. *Curr Protoc Protein Sci* **2004,** *Chapter 3*, Unit 3.1 1-3.1.9..

21. Fonin, A. V.; Sulatskaya, A. I.; Kuznetsova, I. M.; Turoverov, K. K., Fluorescence of dyes in solutions with high absorbance. Inner filter effect correction. *PloS one* **2014,** *9* (7), e103878-e103878.

22. Tsolekile, N.; Nahle, S.; Zikalala, N.; Parani, S.; Sakho, E. H. M.; Joubert, O.; Matoetoe, M. C.; Songca, S. P.; Oluwafemi, O. S., Cytotoxicity, fluorescence tagging and gene-expression study of CuInS/ZnS QDS - meso (hydroxyphenyl) porphyrin conjugate against human monocytic leukemia cells. *Scientific Reports* **2020,** *10* (1), 4936.

23. Kou, J.; Dou, D.; Yang, L., Porphyrin photosensitizers in photodynamic therapy and its applications. *Oncotarget* **2017,** *8* (46), 81591-81603.

24. Sharma, B.; Jain, A.; Pérez-García, L.; Watts, J. A.; Rawson, F. J.; Chaudhary, G. R.; Kaur, G., Metallocatanionic vesicle-mediated enhanced singlet oxygen generation and photodynamic therapy of cancer cells. *Journal of Materials Chemistry B* **2022,** *10* (13), 2160-2170.

25. García Calavia, P.; Bruce, G.; Pérez-García, L.; Russell, D. A., Photosensitiser-gold nanoparticle conjugates for photodynamic therapy of cancer. *Photochem Photobiol Sci* **2018,** *17* (11), 1534-1552.

26. Fisher, W. R.; Taniuchi, H.; Anfinsen, C. B., On the Role of Heme in the Formation of the Structure of Cytochrome c. *Journal of Biological Chemistry* **1973,** *248* (9), 3188-3195.

27. Maiti, N. C.; Mazumdar, S.; Periasamy, N., J- and H-Aggregates of Porphyrin−Surfactant Complexes: Time-Resolved Fluorescence and Other Spectroscopic Studies. *The Journal of Physical Chemistry B* **1998,** *102* (9), 1528-1538.

28. Scolaro, L. M.; Romeo, A.; Castriciano, M. A.; Micali, N., Unusual optical properties of porphyrin fractal J-aggregates. *Chemical Communications* **2005,** (24), 3018-3020.

29. Siggel, U.; Bindig, U.; Endisch, C.; Komatsu, T.; Tsuchida, E.; Voigt, J.; Fuhrhop, J.-H., Photophysical and photochemical properties of porphyrin aggregates. *Berichte der Bunsengesellschaft für physikalische Chemie* **1996,** *100* (12), 2070-2075.

30. Caesar, C. E. B.; Esbjörner, E. K.; Lincoln, P.; Nordén, B., Assigning membrane binding geometry of cytochrome C by polarized light spectroscopy. *Biophys J* **2009,** *96* (8), 3399-3411.

Supporting Information

Molecular Surface Quantification of Multi-Functionalized Gold Nanoparticles Using UV-visible absorption Spectroscopy Deconvolution

Jordan C. Potts, Akhil Jain, David B. Amabilino, Frankie J. Rawson* and Lluïsa Pérez-García*

Jordan C. Potts and Dr. Lluïsa Pérez-García
Division of Advanced Materials and Healthcare Technologies
School of Pharmacy
University of Nottingham, Nottingham NG7 2RD, UK

Dr. Akhil Jain and Dr. Frankie J. Rawson
Bioelectronics Laboratory, Division of Regenerative Medicine and Cellular Therapies
School of Pharmacy, Biodiscovery Institute
University of Nottingham, Nottingham NG7 2RD, UK

Dr. David B. Amabilino
Institut de Ciència de Materials de Barcelona (ICMAB)
CSIC, Carrer dels Til·lers
Campus Universitari, 08193 Cerdanyola del Vallès, Catalunya, Spain

Dr. Lluïsa Pérez-García
Departament de Farmacologia, Toxicologia i Química Terapèutica,
Facultat de Farmàcia i Ciències de l'Alimentació
Universitat de Barcelona, 08028 Barcelona, Spain

Dr. Lluïsa Pérez-García
Institut de Nanociència i Nanotecnologia UB (IN2UB),
Universitat de Barcelona, 08028 Barcelona, Spain

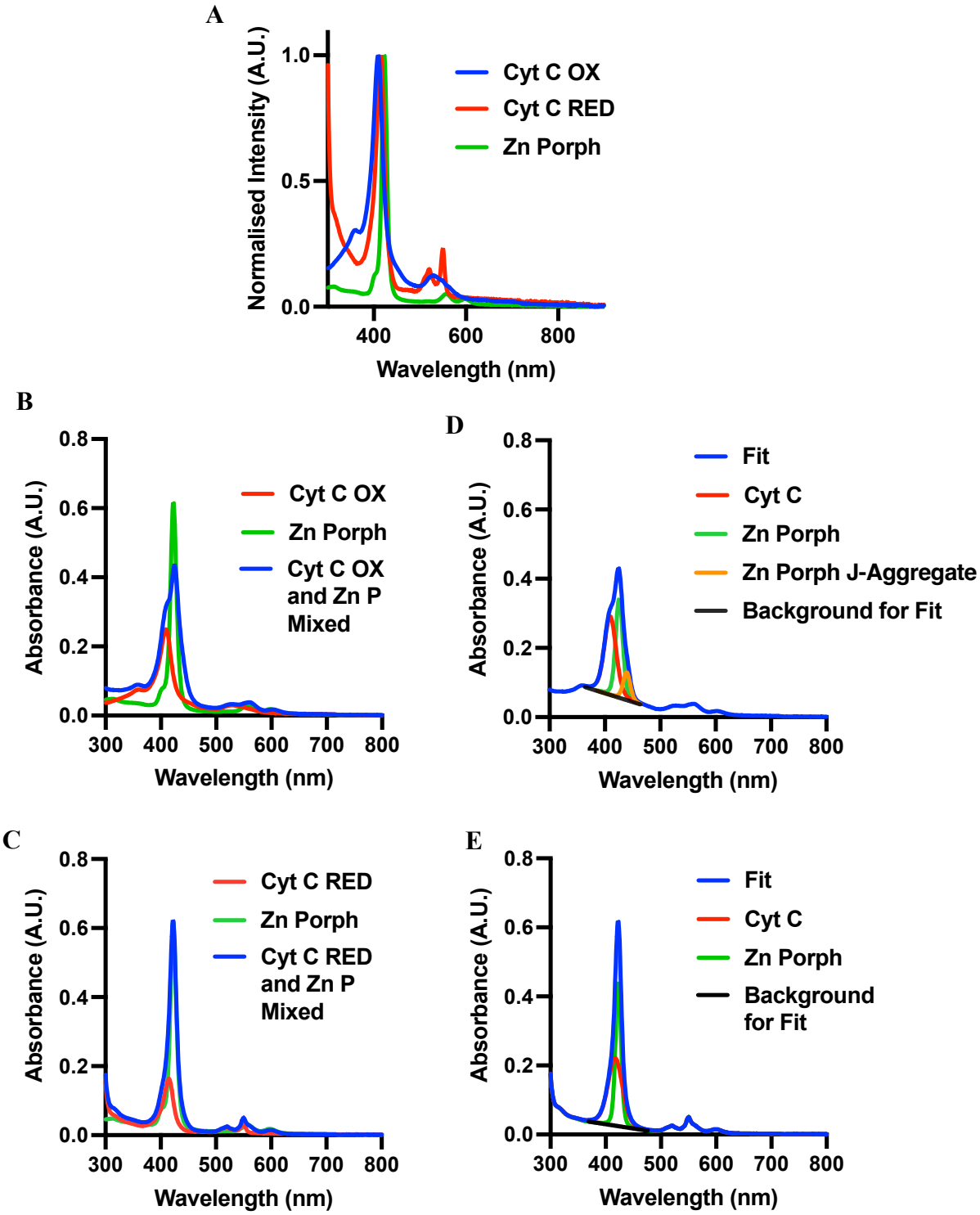

Figure S1. Ultraviolet-Visible absorption spectra of **(A)** Cyt *C* OX, Cyt *C* RED and Zn Porph free in solution with normalized intensity. **(B)** Cyt *C* OX and Zn Porph mixed and independently free in solution at 2.5 mM. **(C)** Cyt *C* RED and Zn Porph mixed and independently free in solution at 2.5 mM. **(D)** Deconvolution and fitted spectra of Cyt *C* OX and Zn Porph mixed to reveal hidden spectra of Cyt *C* and Zn Porph individual components. **(E)** Deconvolution and fitted spectra of Cyt *C* RED and Zn Porph mixed to reveal hidden spectra of Cyt *C* and Zn Porph individual components.

Table S2. AuNP, Cyt *C* and Zn Porph concentration and number of molecules calculated from the UV-visible absorption absorption spectra of Figure 3A and 3B

	AuNP		Cyt *C*			Zn Porph			
Sample	Concentration (nM)	Number of Molecules	Concentration (μM)	Number of Molecules	Number Per AuNP	Zn Porph/Porph Concentration (μM)	Zn Porph/Porph Number of Molecules	Zn Porph/Porph Per AuNP	Free Zn Porph Concentration (μM)
20 nm AuNP-PEG-Cyt *C* /Zn Porph (Figure 3A)	1.21	7.30×10^{14}	0.42	2.53×10^{17}	346	1.30	7.83×10^{17}	1073	-
20 nm AuNP-PEG-Cyt *C* /Zn Porph (Figure 3B)	0.26	1.55×10^{14}	0.40	2.40×10^{17}	1545	1.16	6.99×10^{17}	4500	1.11
50 nm AuNP-PEG-Cyt *C*/Porph(Figure S4A)	0.0096	5.79×10^{12}	0.11	6.73×10^{16}	2 3259	0.17	1.02×10^{17}	35168	

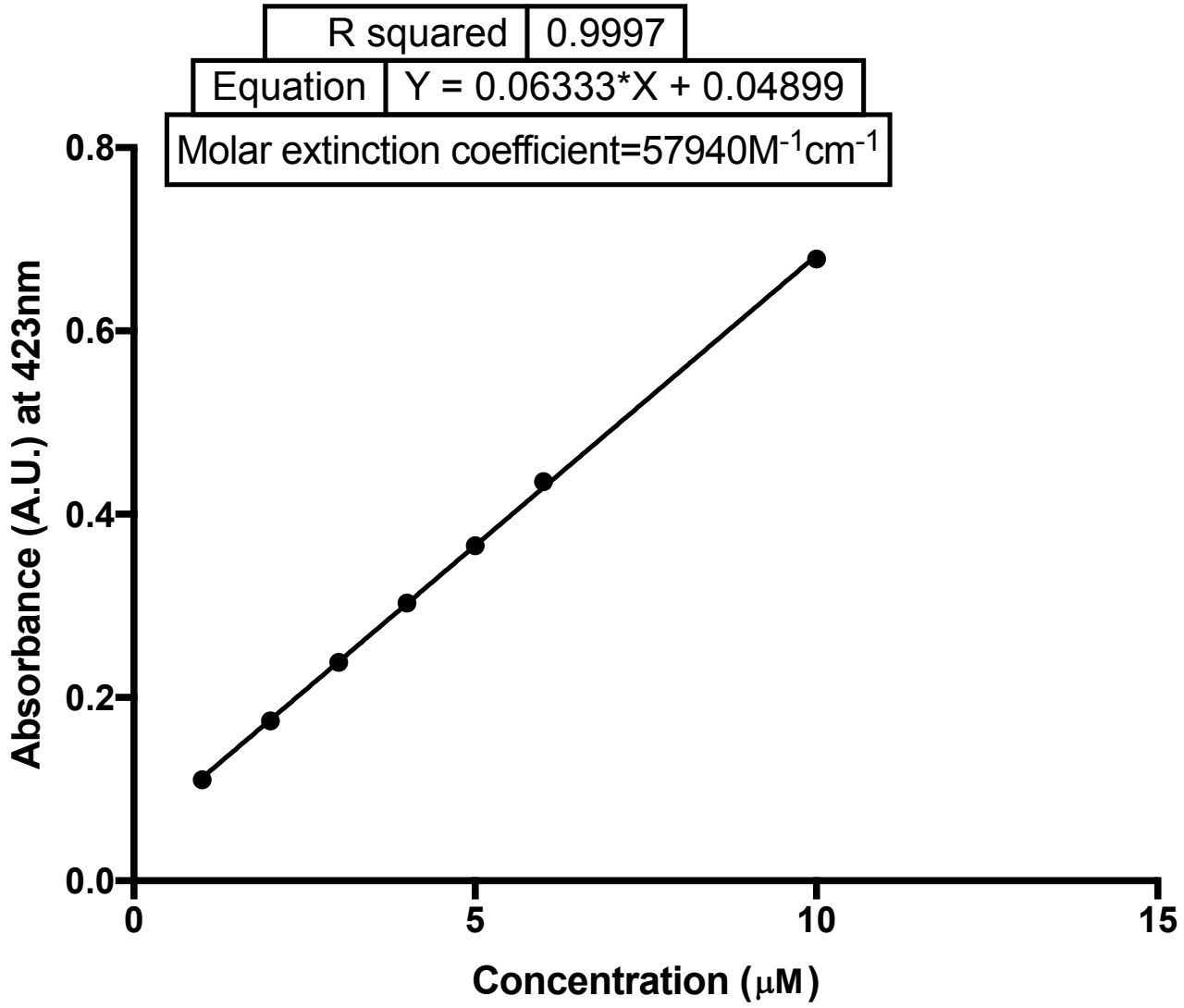

Figure S3. The concentration plot used to calculate the extinction coefficient of Zn Porph

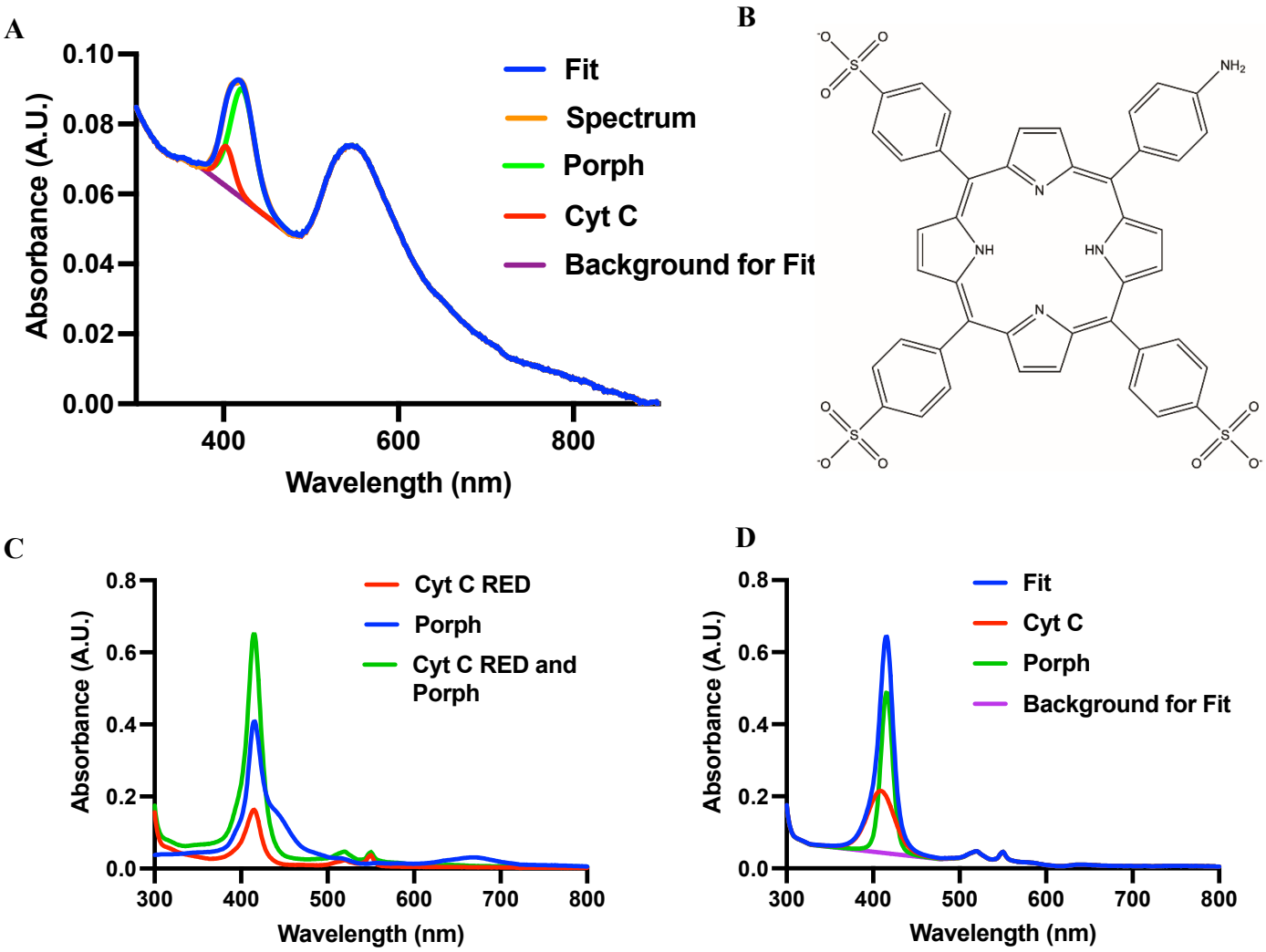

Figure S4. UV-visible absorption absorption spectra of 50 nm AuNP-PEG-Cyt *C*/Porph with Soret band deconvolution **(A)**. Structure of Porph (extinction coefficient 184900 M^{-1} cm^{-1}) **(B)**. UV-visible absorption absorption spectra of Cyt *C* RED, Porph and both mixed free in solution at 2.5µM **(C)**. Deconvolution of UV-visible absorption absorption spectra of Cyt *C* RED and Porph mixed in solution **(D)**.

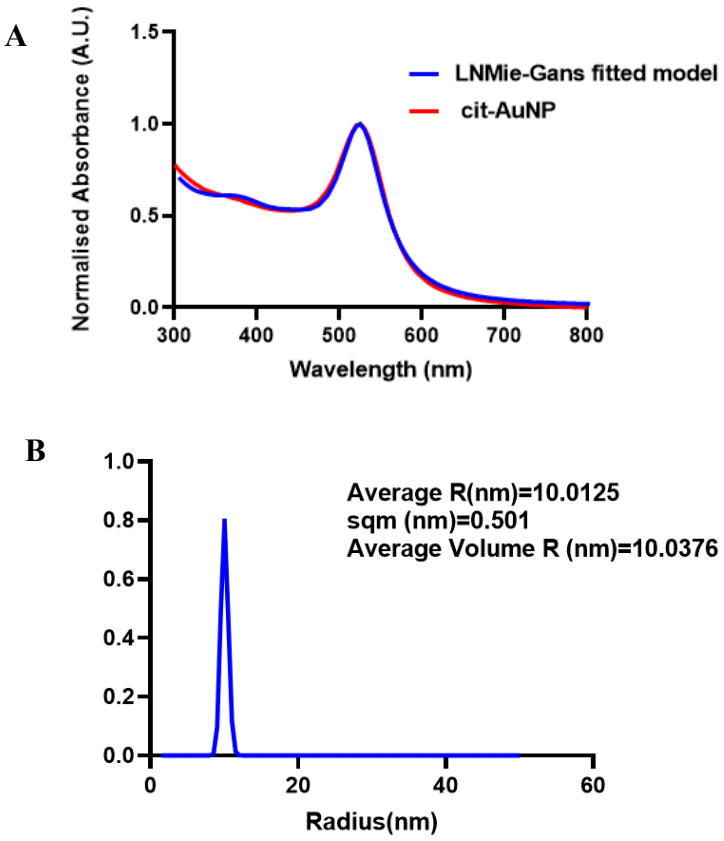

Figure S5. The use of LN-MIE-Gans model fitting to ca. 20 nm cit-AuNPs (A) to predict their size (B).